Coming to Grips with N−H···N Bonds. 2. Homocorrelations between Parameters Deriving from the Electron Density at the Bond Critical Point[1]

Osvald Knop,* Kathryn N. Rankin,† and Russell J. Boyd‡

Department of Chemistry, Dalhousie University, Halifax NS, Canada B3H 4J3

Received: September 24, 2002; In Final Form: November 5, 2002

The equilibrium geometries of 54 small molecules containing linear or near-linear N−H···N bonds (sample **M**) have been optimized at the MP2/6-31G(d,p) level and the values of p' and p'' of the parameters p_c at the bond-critical points (p' in the N−H, p'' in the H···N bond) have been computed from the results of these optimizations. Because the N−H and the H···N part of an N−H···N bond system have different character, the trends of p' and of p'' in **M** are described by different functions. With the p_c as descriptors (the electron density ρ_c, the curvatures $\lambda_{c,i}$, the Laplacian ∇^2_c, the kinetic energy densities G_c and K_c, and the potential energy density V_c), we have searched for correlations of p' and p'' (*homocorrelations*) in **M**. A high degree of correlation has been found for all the parameters. With the exception of the linear ρ',ρ'' correlation the homocorrelations of the other p_c are nonlinear and some of them nonmonotonic. The homocorrelations permit estimates of the p_c values, p_s, in *symmetric* N−H−N bonds, where estimates from experiment are not without problems. They also answer some of the questions concerning limiting values of the p_c. With the exception of G_c, correlations between *unlike* p_c's (heterocorrelations, p',q' and p'',q'') will be reported in a subsequent paper, now in preparation. The heterocorrelations involving G_c are included here because of the prominence of G_c in recent discussion of hydrogen bonds in the literature.

Introduction

In part 1[1,2] we examined correlations between the internuclear distances N−H = d', H···N = d'', and N···N = D in linear or near-linear N−H···N hydrogen bonds present in 67 small molecular species the geometries of which had been optimized at the RHF/6-31G(d,p) level (the HF set **S**), and in 19 of these species with the geometries optimized at the MP2/6-31G(d,p) level (the MP2 set). Also examined were the distances x',x'' between the N and H atoms and the positions of the bond critical points (BCP) in these bonds, and the correlations of the electron density ρ_c at the BCP with d', d'', and D. The resulting correlations appeared to be supported by experiment wherever comparison was possible. The main conclusions of the examination can be summarized as follows:

The position of the proton in linear or near-linear N_d−H···N_a bonds can be estimated from a single parameter, the N···N distance, as can the positions of the critical points in the N_d−H and H···N_a component bonds.

The N_d−H and H···N_a component bonds in a linear or near-linear N_d−H···N_a system do not have the same character. The d,ρ_c correlation curve for the system is continuous but not smooth: the d'',ρ'' part of the curve is separated from the d',ρ' part by a shallow cusp at d_s,ρ_s, i.e., at the point of intersection corresponding to *the* symmetric N−H−N bond.

Linear or near-linear prosymmetric N−H···N bonds with short N···N separations, expected to optimize to yield symmetric N−H−N bonds, do so when optimized in MP2/6-31G(d,p) but not when optimized in HF/6-31G(d,p); instead, an asymmetric N−H···N bond results. The bond-critical parameters in these asymmetric bonds have values that fit in well with those obtained from all the other asymmetric, nonprosymmetric N−H···N bonds similarly optimized.

In part 2 we now examine homoparametric relationships (*homocorrelations* for short) between p', p'', where p' refers to the N−H and p'' to the H···N bond in a linear or near-linear N−H···N system, and p stands for one of the parameters at the BCP: the electron density ρ_c, the curvatures $\lambda_{12,c}$ and $\lambda_{3,c}$ (see Notation below), the Laplacian ∇^2_c, and the potential (V_c) and kinetic (G_c, K_c) energy densities. With the exception of d',d'' correlations,[1,3−8] these relationships, for N−H···N or for that matter any X−H···X hydrogen-bonded systems, do not appear to have been investigated previously, either by theoretical calculation or by experiment.

Housekeeping

Notation. The notation follows that of part 1. For symmetric N−H−N bonds, $p' = p'' = p_s$. As in part 1, the symbols ∇^2_c, $\nabla^2\,'$, and $\nabla^2\,''$ are shorthand for $\nabla^2(\rho_c)$, $\nabla^2(\rho_c')$ (at the BCP X′ in the N_d−H bond), and $\nabla^2(\rho_c'')$ (at the BCP X″ in the H···N bond), respectively. For convenience we recall that $\lambda_{12} = {}^1/_2(\lambda_1 + \lambda_2)$ and $\nabla^2 = \Sigma\lambda_i = 2\lambda_{12} + \lambda_3$. Definitions of the bond-critical parameters and descriptions of their formal properties will be found in refs 9 and 10.

The goodness of fit of a regression $y = R(x)$ is judged, apart from the (generalized) r^2, by the standard deviation $\sigma_f = (\Sigma\Delta^2/f)^{1/2}$ for f degrees of freedom as such *and* as percent of the range of the dependent variable y (e.g., $\sigma_{52} = 0.244-0.8\%$), and also by the uniformity of distribution of the residuals.

Data Sets. The RHF/6-31G(d,p) sample **S** of part 1 has been left unchanged, but the rather lacunary set of the 19 MP2/6-

* To whom correspondence should be addressed. Fax: (902) 494-1310. E-mail: chemistry@dal.ca.

† Present address: Biotechnology Research Institute, National Research Council of Canada, 6100 av. Royalmount, Montreal, Que., Canada H4P 2R2. E-mail: kathryn.rankin@bri.nrc.ca.

‡ E-mail: russell.boyd@dal.ca.

10.1021/jp022127b CCC: $25.00
Published on Web 12/12/2002

TABLE 1: MP2/6-31G(d,p) Optimized Equilibrium Molecular Geometries[a]

	configuration	PG	N_dHN_a	$-E$	$-E_f$	$\epsilon(N_d)$	$\epsilon(H)$	$\epsilon(N_a)$
5	$[OCNH\cdots NCO]^-$	C_s	179.5	335.938523	0.04872	−0.762	0.541	−0.776
6	$[HCNH\cdots NCF]^+$	$C_{\infty v}$	(180)	285.645702	0.04645	−0.481	0.601	−0.487
15	$[FCNH\cdots NCCN]^+$	C_s	180.0	377.619743	0.03683	−0.311	0.519	−0.448
9a	$[NCCNH\cdots NF_3]^+$	C_{3v}	(180)	538.661028	0.01660	−0.460	0.530	0.605
9b	$[F_3NH\cdots NCCN]^+$	C_{3v}	(180)	538.661032	0.04533	−0.624	0.525	−0.466
13	$[CNH\cdots NCO]^-$	$C_{\infty v}$	(180)	260.849193	0.05593	−0.581	0.514	−0.761
16	$[HCNH\cdots NCCN]^+$	$C_{\infty v}$	(180)	278.641419	0.03534	−0.309	0.503	−0.449
18	$[OCNH\cdots NNN]^-$	C_s	177.4	332.064737	0.04413	−0.733	0.487	−0.668
14	$[H_3NH\cdots NCLi]^+$	C_{3v}	(180)	156.868280	0.07460	−0.703	0.436	−0.428
1	$[FCNH\cdots NF_3]^+$	C_{3v}	(180)	545.668289	0.01611	−0.303	0.512	0.577
22	$[CNH\cdots NCS]^-$	$C_{\infty v}$	(180)	583.454071	0.04335	−0.562	0.487	−0.641
39	NNNH···NCS	C_s	178.5	654.663214	0.03568	−0.565	0.474	−0.644
25	$[OCNH\cdots NCS]^-$	C_s	179.6	658.543491	0.03623	−0.569	0.402	−0.481
37	$[HCNH\cdots NF_3]^+$	C_{3v}	(180)	446.690182	0.01484	−0.302	0.491	0.577
27	$[LiCNH\cdots NCH]^+$	C_s	179.9	193.628849	0.03063	−0.335	0.433	−0.352
29	$[LiCNH\cdots NCF]^+$	$C_{\infty v}$	(180)	292.610593	0.02786	−0.334	0.432	−0.350
26	SCNH···NCLi	C_s	179.5	590.893752	0.02314	−0.480	0.379	−0.372
33	$[H_3NH\cdots NCH]^+$	C_{3v}	(180)	149.935394	0.03554	−0.671	0.426	−0.379
34	$[H_3NH\cdots NCF]^+$	C_{3v}	(180)	248.916891	0.03252	−0.669	0.428	−0.380
38	$[LiCNH\cdots NCCN]^+$	$C_{\infty v}$	(180)	285.609731	0.02018	−0.332	0.424	−0.408
36	$CNH\cdots NH_3$	C_{3v}	(180)	149.539466	0.02206	−0.389	0.391	−0.788
35	CNH···NCLi	$C_{\infty v}$	(180)	193.218218	0.02403	−0.558	0.440	−0.502
40	$[H_3NH\cdots NCCN]^+$	C_{3v}	(180)	241.914489	0.02330	−0.666	0.423	−0.434
43	OCNH···NCLi	C_s	179.4	268.309813	0.01909	−0.711	0.423	−0.501
49	NNNH···NCLi	C_s	177.2	264.429630	0.01863	−0.523	0.405	−0.501
47	CNH···NCH	$C_{\infty v}$	(180)	186.312984	0.01262	−0.372	0.365	−0.319
45	SCNH···NCH	C_s	179.3	583.988170	0.01138	−0.497	0.363	−0.319
48	CNH···NCF	$C_{\infty v}$	(180)	285.296451	0.01157	−0.372	0.365	−0.317
56	$[LiCNH\cdots NF_3]^+$	C_{3v}	(180)	453.666145	0.00733	−0.330	0.401	0.618
46	SCNH···NCF	C_s	179.6	682.971710	0.01040	−0.650	0.413	−0.406
54	CNH···NCCN	$C_{\infty v}$	(180)	278.300357	0.00865	−0.372	0.360	−0.356
50	SCNH···NCCN	C_s	178.7	675.975906	0.00777	−0.501	0.355	−0.355
55	OCNH···NCF	C_s	179.5	360.390306	0.00889	−0.574	0.353	−0.318
58	NNNH···NCH	C_s	179.1	257.526500	0.00933	−0.507	0.375	−0.420
60	NNNH···NCF	C_s	177.6	356.510275	0.00858	−0.505	0.373	−0.403
57	OCNH···NCCN	C_s	178.2	353.394855	0.00662	−0.701	0.385	−0.451
63	$CNH\cdots NF_3$	C_{3v}	(180)	446.364308	0.00334	−0.559	0.381	0.825
62	$SCNH\cdots NF_3$	C_s	179.3	844.040536	0.00314	−0.502	0.331	0.655

[a] This table contains MP2/6-31G(d,p) optimized species added to those of Table 3 of ref 1; the species listed there and those in the above table constitute sample **M**. The numbering is as in ref 1; some species listed there do not appear in the above table as they could not be successfully optimized in MP2/6-31G(d,p). Numbers **9a** and **9b** correspond to **9** of ref 1: they differ in the mode of protonation. N_dHN_a bond angle (deg), total electronic energy E (au), energy of formation E_f from component parts (au), and net atom charges ϵ (Mulliken, e) are arranged in the order of increasing D.

31G(d,p) optimizations in part 1 has been augmented by 35 additional optimizations (Tables 1 and 2). This brings the MP2 set to a total of 54 optimizations that constitute sample **M**. The numbering of these additional MP2-optimized species follows that of Table 1 in part 1. The point groups PG correspond to the lowest energy HF conformations in part 1.

In the following, all the correlations are based on the augmented MP2 set **M**. Whereas the number of chemical species in the HF set of part 1 matches **M**, the homocorrelations for that set, although examined, are not described here, as optimization at the HF/6-31G(d,p) level does not lead to symmetric N−H−N bonds from prosymmetric N−H···N bonds (cf. Introduction) and the HF set is thus deficient in a data domain of crucial importance in the present investigation.

The dimensions of all the bond parameters are in au (d and D in Å) and are self-consistent. To obtain an idea of the magnitude of the combined error due to rounding off, to merging λ_1 and λ_2 to λ_{12}, and to other, unspecified or unidentified sources, we tested the equations $K_c - G_c + (1/4)\nabla^2_c = \delta$ and $2\lambda_{12} + \lambda_3 - \nabla^2_c = \delta$, for which $\delta = 0$ by definition. In the first case, $-0.0010 < \delta < 0.007$ and $-0.0006 < \delta < 0.004$ for p' and p'', respectively; in the second case, $-0.0002 < \delta < 0.005$ and $-0.0002 < \delta < 0.003$, i.e., in both cases values that can be neglected for our purposes except for $p'' = K''$ (for which see below).

Bond-Critical Parameter Correlations: General Information

The degree of association of the three atoms in a complete $N_d-H\cdots N_a$ bond (i.e., in a quasi-isolated $N_d-H\cdots N_a$ system) can be assessed by the strength of the correlation of a BCP parameter p' in the N_d-H bond with the corresponding parameter p'' in the $H\cdots N_a$ bond, i.e., by the strength of the p', p'' *homocorrelation*. For the bond lengths d',d'' and the distances x',x'' to the BCPs the homocorrelations have been investigated previously,[1,3] utilizing an extension of Pauling's bond-order equation to linear or near-linear 3c4e systems. For the d',d'' relationship the applicability of this model has been verified by comparison with bond lengths obtained from standard crystal-structure determinations by neutron diffraction or careful X-ray diffraction. For other BCP parameters, however, appropriate theory-based (or at least semiempirical) model functions appear to be lacking, and empirical homocorrelations of our ab initio results are more difficult to verify because of the paucity of detailed and reliable experimental electron-density distributions in suitable N−H···N containing species. The MP2 p', p'' dependences described in the following have therefore been treated statistically, exploring phenomenological model functions with properties compatible with the physical characteristics of p' and p'' (boundary conditions etc.).

TABLE 2: Internuclear and Atom···BCP Distances (Å), Electron Densities $\rho_c(r)$, Laplacians $\nabla^2\rho_c(r)$, Eigenvalues λ_i of the Laplacians, Ellipticities η, and Kinetic Energy Densities $G(r)$ and $K(r)$ at the Bond-Critical Points (All in au) in the MP2/6-31G(d,p) Optimized Species of Table 1 (Arranged in the Order of Increasing D)[a]

	D	d';d''	x';x''	ρ';ρ''	λ_{12}';λ_{12}''	λ_3';λ_3''	η	∇^2';∇^2''	G';G''	K';K''
5	2.516	1.208	0.954	0.1712	−0.5960	0.5859	0.000	−0.6062	0.0632	0.2147
		1.308	0.991	0.1286	−0.3712	0.5161	0.001	−0.2263	0.0658	0.1224
6	2.540	1.162	0.944	0.1974	−0.8272	0.7932	0	−0.8611	0.0544	0.2700
		1.378	1.028	0.1041	−0.2881	0.5116	0	−0.0646	0.0615	0.0777
15	2.546	1.157	0.918	0.2012	−0.7747	0.7064	0.000	−0.8430	0.0612	0.2720
		1.389	1.018	0.1068	−0.2850	0.5140	0.000	−0.0561	0.0598	0.0738
9a	2.548	1.258	0.951	0.1606	−0.5272	0.5950	0	−0.4593	0.0642	0.1791
		1.290	0.985	0.1578	−0.4975	0.5870	0	−0.4080	0.0695	0.1715
9b	2.549	1.232	0.961	0.1884	−0.6766	0.6448	0	−0.7085	0.0636	0.2407
		1.317	0.974	0.1344	−0.3883	0.5763	0	−0.2003	0.0681	0.1182
13	2.569	1.123	0.916	0.2252	−0.9811	0.8707	0	−1.0915	0.0501	0.3229
		1.446	1.051	0.0863	−0.2032	0.4703	0	0.0639	0.0582	0.0423
16	2.580	1.124	0.902	0.2248	−0.9329	0.8209	0	−1.0449	0.0559	0.3171
		1.456	1.048	0.0888	−0.2160	0.4712	0	0.0391	0.0538	0.0440
18	2.609	1.103	0.890	0.2380	−0.9946	0.8307	0.001	−1.1584	0.0518	0.3414
		1.507	1.077	0.0779	−0.1659	0.4174	0.031	0.0856	0.0496	0.0282
14	2.612	1.122	0.892	0.2455	−0.9739	0.7776	0	−1.1702	0.0576	0.3501
		1.490	1.055	0.0858	−0.1921	0.4626	0	0.0784	0.0537	0.0341
1	2.630	1.111	0.886	0.2329	−0.9553	0.8242	0	−1.0865	0.0584	0.3300
		1.519	1.092	0.0846	−0.2058	0.4514	0	0.0398	0.0473	0.0374
22	2.664	1.068	0.872	0.2688	−1.2535	1.0082	0	−1.4987	0.0408	0.4147
		1.596	1.124	0.0580	−0.1121	0.3586	0	0.1344	0.0427	0.0091
39	2.666	1.088	0.874	0.2685	−1.1307	0.8385	0.019	−1.4229	0.0434	0.3991
		1.578	1.105	0.0623	−0.1212	0.3847	0.010	0.1423	0.0461	0.0105
25	2.673	1.067	0.850	0.2675	−1.1119	0.8661	0.004	−1.3578	0.0554	0.3948
		1.606	1.115	0.0601	−0.1120	0.3452	0.003	0.1213	0.0406	0.0103
37	2.686	1.088	0.873	0.2534	−1.0954	0.9150	0	−1.2759	0.0520	0.3710
		1.598	1.130	0.0680	−0.1494	0.3801	0	0.0813	0.0394	0.0191
27	2.743	1.046	0.840	0.2884	−1.2968	1.0128	0.000	−1.5808	0.0458	0.4410
		1.697	1.165	0.0464	−0.0809	0.2774	0.000	0.1156	0.0317	0.0028
29	2.755	1.041	0.836	0.2926	−1.3195	1.0220	0	−1.6170	0.0449	0.4491
		1.714	1.170	0.0431	−0.0725	0.2601	0	0.1150	0.0302	0.0014
26	2.795	1.033	0.820	0.2977	−1.2740	0.9493	0.002	−1.5985	0.0522	0.4519
		1.762	1.195	0.0406	−0.0636	0.2361	0.002	0.1088	0.0279	0.0007
33	2.809	1.052	0.835	0.3035	−1.2900	0.9166	0	−1.6639	0.0458	0.4616
		1.757	1.187	0.0417	−0.0666	0.2434	0	0.1102	0.0285	0.0010
34	2.814	1.049	0.832	0.3062	−1.3018	0.9193	0	−1.6844	0.0453	0.4664
		1.765	1.187	0.0398	−0.0620	0.2338	0	0.1098	0.0278	0.0004
38	2.816	1.034	0.828	0.3001	−1.3528	1.0305	0	−1.6751	0.0439	0.4626
		1.782	1.207	0.0368	−0.0577	0.2185	0	0.1031	0.0255	−0.0003
36	2.835	1.033	0.822	0.3020	−1.3067	0.9717	0	−1.6417	0.0501	0.4605
		1.801	1.233	0.0423	−0.0646	0.2274	0	0.0982	0.0275	0.0030
35	2.842	1.026	0.828	0.3097	−1.4367	1.0626	0	−1.8109	0.0358	0.4885
		1.816	1.235	0.0331	−0.0490	0.2063	0	0.1083	0.0250	−0.0021
40	2.876	1.044	0.826	0.3115	−1.3193	0.9149	0	−1.7236	0.0447	0.4756
		1.832	1.224	0.0344	−0.0504	0.1972	0	0.0963	0.0237	−0.0004
43	2.904	1.024	0.816	0.3122	−1.3562	0.9510	0.003	−1.7613	0.0414	0.4817
		1.880	1.263	0.0290	−0.0396	0.1743	0.006	0.0951	0.0217	−0.0020
49	2.932	1.036	0.814	0.3215	−1.3200	0.8386	0.026	−1.8015	0.0428	0.4932
		1.896	1.260	0.0292	−0.0394	0.1725	0.020	0.0937	0.0220	−0.0014
47	3.002	1.009	0.795	0.3262	−1.4013	0.9901	0	−1.8125	0.0490	0.5021
		1.993	1.307	0.0229	−0.0291	0.1274	0	0.0692	0.0166	−0.0007
45	3.012	1.013	0.793	0.3203	−1.3263	0.9148	0.003	−1.7380	0.0539	0.4884
		1.999	1.309	0.0228	−0.0287	0.1253	0.004	0.0681	0.0163	−0.0007
48	3.013	1.008	0.793	0.3275	−1.4032	0.9870	0	−1.8193	0.0491	0.5040
		2.005	1.308	0.0217	−0.0269	0.1210	0	0.0672	0.0160	−0.0008
56	3.016	1.020	0.812	0.3144	−1.3990	1.0297	0	−1.7683	0.0438	0.4858
		1.996	1.329	0.0242	−0.0334	0.1321	0	0.0654	0.0157	−0.0007
46	3.025	1.011	0.801	0.3249	−1.4041	0.9638	0.002	−1.8443	0.0412	0.5023
		2.014	1.322	0.0199	−0.0242	0.1171	0.004	0.0686	0.0155	−0.0016
54	3.073	1.005	0.789	0.3303	−1.4058	0.9789	0	−1.8327	0.0499	0.5080
		2.068	1.341	0.0191	−0.0231	0.1046	0	0.0584	0.0140	−0.0006
50	3.093	1.009	0.786	0.3247	−1.3229	0.8905	0.004	−1.7553	0.0556	0.4944
		2.085	1.347	0.0187	−0.0222	0.1008	0.004	0.0564	0.0136	−0.0005
55	3.097	1.010	0.784	0.3249	−1.2999	0.8559	0.008	−1.7440	0.0578	0.4938
		2.087	1.342	0.0186	−0.0217	0.1003	0.006	0.0568	0.0137	−0.0005
58	3.128	1.024	0.791	0.3355	−1.3229	0.7744	0.032	−1.8713	0.0469	0.5147
		2.104	1.352	0.0181	−0.0212	0.1013	0.020	0.0588	0.0139	−0.0008
60	3.141	1.023	0.790	0.3364	−1.3207	0.7669	0.032	−1.8744	0.0474	0.5160
		2.118	1.353	0.0172	−0.0198	0.0965	0.020	0.0569	0.0134	−0.0008
57	3.163	1.009	0.788	0.3319	−1.3601	0.8708	0.005	−1.8494	0.0464	0.5087
		2.155	1.386	0.0150	−0.0171	0.0851	0.008	0.0508	0.0118	−0.0010
63	3.284	1.000	0.789	0.3382	−1.4711	1.0000	0	−1.9422	0.0395	0.5250
		2.284	1.469	0.0116	−0.0135	0.0659	0	0.0389	0.0088	−0.0009
62	3.320	1.006	0.776	0.3293	−1.3085	0.8497	0.004	−1.7672	0.0585	0.5003
		2.314	1.470	0.0122	−0.0138	0.0646	0.004	0.0369	0.0086	−0.0006

[a] See footnote of Table 1.

TABLE 3: Summary of Bond-Critical Parameters p_s in Symmetric N−H−N Bonds

	p_s from			p_s mean[a]	
parameter	regression	eq	N−H−N[b]	unweighted	weighted
ρ_s	0.152(7)	1	0.152(4)	0.152	0.152
$\lambda_{12,s}$	−0.502(36)	2c	−0.493(8)	−0.497	−0.493
$\lambda_{3,s}$	0.571(44)	3b	0.560(10)	0.565	0.560
∇^2_s	−0.423(16)	4	−0.425(9)	−0.424	−0.425
G_s	0.060(3)	5a	0.066(2)	0.063	0.065
K_s	0.173(4)	6a	0.172(2)	0.172	0.172
V_s	−0.241(11)	7	−0.238(3)	−0.239	−0.238

[a] Mean of p_s from columns 2 and 4. [b] Mean p_s from the symmetric N−H−N bonds **2**−**4**, **10**, and **11** (Table 4 in part 1).

TABLE 4: Position of the Transition from Closed-Shell to Shared Bond Interactions in Diatomic XH Hydrides[a]

from[b]	X from 1st row[c]	X from 2nd row[c]	figure
	Evaluation from Trends in Ref 9		
sign of ϵ(H)	**Li Be B C** *N O F*	**Na Mg Al Si P S** *Cl*	6.2[d]
ρ_c contours	**Li Be B** *C N O F*	**Na Mg Al Si P** *S Cl*	6.3[d]
∇^2_c contours	**Li Be B** *C N O F*	**Na Mg Al Si** *P S Cl*	7.19[d]
	Evaluation from This Work		
G_c, ln($-V_c$)	**Li Be** ? *C N O F*	**Na Mg Al Si P** ? ?	16A
ρ_c,G_c/V_c	**Li Be** ? *C N O F*	**Na Mg Al Si P** *S Cl*	17B
ρ_c, [($d_c - x_c$)/d_c]	**Li Be B** *C N O F*	**Na Mg Al Si P** *S Cl*	17A
ρ_c,V_c	**Li Be B** *C N O F*	**Na Mg Al Si P** *S Cl*	
ρ_c, G_c/ρ_c	**Li Be** *B C N O F*	**Na Mg Al Si** ? *S Cl*	11

[a] Based on bond-critical parameters of ref 9; see text. [b] Evaluation from a plot (plots) or from a correlation; ϵ(H), atom charge on H, d_c = d(X−H), x_c = d(H···BCP). [c] Bold type, closed-shell interaction; italic, shared interaction; ?, attribution not obvious. [d] Reference 9.

In *heterocorrelations* the bond-critical parameters being correlated are different in kind, as, for example, d',ρ' and d'',ρ'' in part 1. Here again, verification for N−H···N bonds from experiment is possible only exceptionally at present and one has to rely on the internal consistency of the correlation results. With the exception of $p_c = G_c$ and V_c, heterocorrelations will be dealt with in a subsequent paper.

Homocorrelations

Electron Densities ρ' and ρ''. A ρ'',ρ' plot strongly suggests that the correlation is high and linear. Indeed,

$$\rho' = 0.3506 - 1.302\rho'' \quad (1)$$

$r^2 = 0.983$, $\sigma_{52} = 0.0082-4.3\%$ (when referred to ρ'',($\rho'' - \rho'$), $r^2 = 0.994$, $\sigma_{52} \sim 2.5\%$), with a reasonably uniform distributions of the residuals; $\rho_s = 0.152$. Transforming the variables as (1/ρ''),(ρ'/ρ'') resulted in a linear regression

$$\rho'/\rho'' = -1.1985 + 0.3467/\rho'' \quad (1a)$$

$r^2 = 0.999$, $\sigma_{52} = 0.244-0.8\%$, confirming the validity of (1) but with the residuals increasing with $1/\rho''$. Other monotonic model functions tried did not improve on the linear regression.

The $\rho_s = 0.152(8)$ value from (1) agrees well with the estimate $\rho_s = 0.150$ obtained via a d_c,ρ_c regression (eq 8f in part 1) and with the mean 0.152(4) of the five $\rho' = \rho''$ values for the symmetric bonds (**2**−**4**, **10**, and **11** in Table 4 of part 1).

Curvatures λ_{12}' and λ_{12}''. These are both negative over the entire data range. The plot of $-\lambda_{12}'$ vs $-\lambda_{12}''$ (Figure 1) does not give a clear indication of what model function might be appropriate. The main problem is posed by the ill-defined cluster

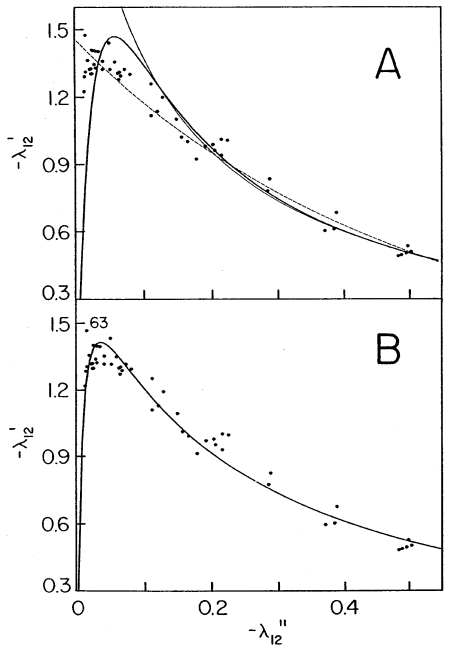

Figure 1. Correlation of the $\lambda_{12,c}$ curvatures. (A) Fitted curves from the exponential regression (2) (broken line) and as obtained via regressions (2b) (thin line) and (2a) (thick line). (B) Fitted curve as obtained via regression (2c). The thick-line curves pass through the origin (see text).

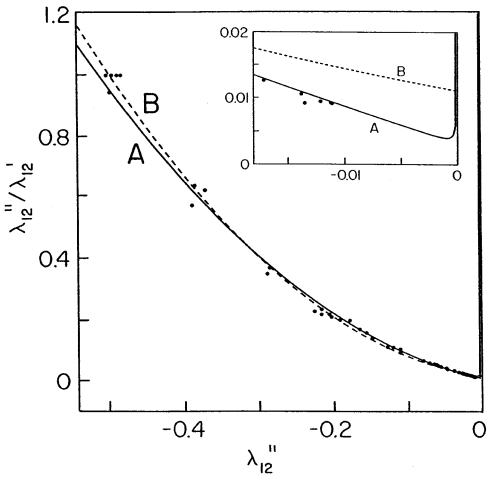

Figure 2. Correlation of the $\lambda_{12,c}$ curvatures. Fitted curves from regression (2a) (B, broken line) and as obtained via regression (2c) (A, solid line). Inset: expansion close to $\lambda_{12}'' = 0$. The minimum of (A) falls at $\lambda_{12}'' = -0.0009$ and $\lambda_{12}''/\lambda_{12}' = 0.0040-0.4\%$, i.e., beyond the data points for the weakest N−H···N bonds. Regression (2c) thus represents the data set adequately.

of points at low $|\lambda_{12}''|$ values. The *gross* trend of $|\lambda_{12}'|$ beyond ~0.03 can be rendered by

$$-\lambda_{12}' = 1.4472 \exp[-2.1211(-\lambda_{12}'')] \quad (2)$$

$r^2 \sim 1.0$, $\sigma_{52} = 0.068-6.8\%$, $\lambda_{12,s} = -0.501$ (Figure 1A, broken line).

To get a better indication of what the "true" model function might be, the behavior of the ratio $\lambda_{12}''/\lambda_{12}'$ was examined (Figure 2, curve B):

$$\lambda_{12}''/\lambda_{12}' = 0.0111-0.2936\lambda_{12}'' + 3.4065(\lambda_{12}'')^2 \quad (2a)$$

$r^2 = 0.997$, $\sigma_{51} = 0.018-1.8\%$, with a $\lambda_{12}''/\lambda_{12}'$ minimum of 0.005 at $\lambda_{12}'' = 0.043$ and $\lambda_{12,s} = -0.497$. Constraining the

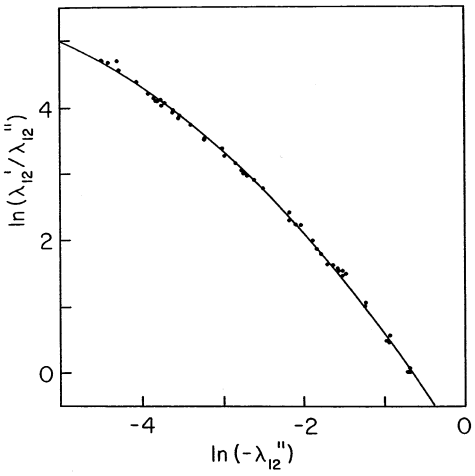

Figure 3. Correlation of the $\lambda_{12,c}$ curvatures. Fitted curve from regression (2c).

regression line to pass through the origin gave essentially the same result:

$$\lambda_{12}''/\lambda_{12}' = -0.4064\lambda_{12}'' + 3.2135(\lambda_{12}'')^2 \qquad (2b)$$

$r^2 \sim 1.0$, $\sigma_{50} = 0.019-1.9\%$, $\lambda_{12,s} = -0.498$.

Clearly, (2a) and (2b) both appear to be good approximations to the data set. When $-\lambda_{12}'$ is expressed from (2a) and plotted in Figure 1A (thick line), the resulting curve accommodates the data points in principle satisfactorily even though its maximum is not well placed, whereas a similar curve from (2b) is an unacceptable fit (Figure 1A, thin line). It thus seems that improving the $\lambda_{12}''/\lambda_{12}'$ fit from (2a) (but not from (2b)) would result in a more faithful representation of the data points in Figure 1. To this end, Figure 2 was replotted logarithmically and quadratic regression was applied (Figure 3):

$$\ln(\lambda_{12}'/\lambda_{12}'') = -1.237 - 1.939\ln(-\lambda_{12}'') - 0.1389[\ln(-\lambda_{12}'')]^2 \qquad (2c)$$

$r^2 = 0.998$, $\sigma_{51} = 0.060-1.3\%$, $\lambda_{12,s} = -0.512$; the fit obtained from (2c) is shown as curve A in Figure 2. Expressing $-\lambda_{12}'$ from (2c) in terms of λ_{12}'' gave $\sigma_{51} = 0.064-6.5\%$, with $(-\lambda_{12}')_{max} = 1.418$ at $-\lambda_{12}'' = 0.034$ (Figure 1B). Given the natural variance of the data set, further improvements in the $-\lambda_{12}'',-\lambda_{12}'$ fit are likely to be largely cosmetic.

The $-\lambda_{12}'',-\lambda_{12}'$ fits obtained from (2) and (2c), respectively, have almost the same σ, also as percent of range. The distribution of the residuals is reasonably uniform and not greatly more so in Figure 1B than that from regression (2). However, there is a fundamental difference between the two fits. The exponential curve from (2) is monotonic and does not pass through the origin (its $-\lambda_{12}'$ at $-\lambda_{12}'' = 0$ is the largest in the data domain), whereas the curve from (2c) passes through the origin (inflection at $-\lambda_{12}'' = 0.0004$, $-\lambda_{12}' = 0.095$) and *has a maximum*, at $-\lambda_{12}'' = 0.341$. Which of the two is the more appropriate is difficult to decide on the present evidence, but it should be noted that regression curves with local extrema inside the data rage, similar to that from (2c), are encountered also, for example, with G_c and may correspond to the real variation of the parameters.

Curvatures λ_3' and λ_3''. Plotting λ_3' against λ_3'' results, unexpectedly, in a confused, quasi-parabolic trend with considerable scatter (Figure 4A). The trend is not improved in logarithmic plots. Quadratic regression (Figure 4A, broken line) gave

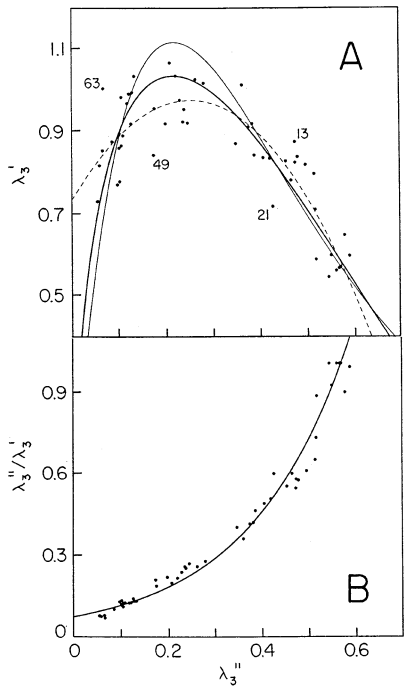

Figure 4. Correlation of the $\lambda_{3,c}$ curvatures. (A) Fitted curve from the quadratic regression (3) (broken line) and as obtained via regressions (3a) (thin line) and (3b) (thick line). (B) Fitted curve from regression (3a).

$$\lambda_3' = 0.729 + 1.937\lambda_3'' - 3.877(\lambda_3'')^2 \qquad (3)$$

($r^2 = 0.772$, $\sigma_{51} = 0.070-13\%$) with a very uniform distribution of the residuals. The λ_3' maximum was located at $\lambda_3'' = 0.250$; $\lambda_3' = 0$ at $\lambda_3'' = -0.251$ and 0.750, i.e., outside the λ_3'' range, and $\lambda_{3,s} = 0.571$.

The variation of the *ratio* λ_3''/λ_3' or λ_3'/λ_3'' with λ_3'' is monotonic, the ratio increasing with λ_3'' in the first and decreasing with increasing λ_3'' in the second case. The *gross* trend in the $\lambda_3'',(\lambda_3''/\lambda_3')$ plot (Figure 4B) could be represented by an exponential regression,

$$\lambda_3''/\lambda_3' = 0.0709\exp(4.659\lambda_3'') \qquad (3a)$$

($\sigma_{52} = 0.050-5.4\%$, $\lambda_{3,s} = 0.568$); note that the regression curve does not pass through the origin.

Expressing λ_3' from (3a) results in the thin solid curve in Figure 4A, which does not pass through the origin: $\sigma_{52} = 0.110-21\%$, with a less uniform distribution of the residuals and with a λ_3' maximum of 1.113 at $\lambda_3'' = 0.215$ and $\lambda_{3,s} = 0.568$. A further improvement was achieved by logarithmic fitting (Figure 5S):

$$\ln(\lambda_3'/\lambda_3'') = 0.9033 + 1.5434\ln(-\ln\lambda_3'') \qquad (3b)$$

$r^2 = 0.988$, $\sigma_{52} = 0.094-3.5\%$, $\lambda_{3,s} = 0.573$. Expressing λ_3' from this regression yielded the thick solid curve in Figure 4A, for which $\sigma_{52} = 0.056-15\%$, with a λ_3' maximum of 1.030 at $\lambda_3'' = 0.214$ and a very uniform distribution of the residuals, though perhaps less so than for (3). This regression curve appears to have the correct functional form; the large natural variation in the sample seems unlikely to be conducive to significant further improvements in the fit.

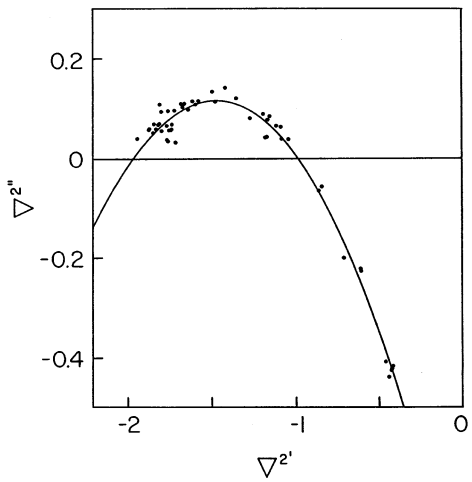

Figure 6. Correlation of the Laplacians ∇^2_c. Fitted curve from the quadratic regression (4).

Laplacians $\nabla^{2\prime}$ and $\nabla^{2\prime\prime}$. An excellent quadratic fit was obtained for the $\nabla^{2\prime},\nabla^{2\prime\prime}$ plot (Figure 6):

$$\nabla^{2\prime\prime} = -0.9451 - 1.440\nabla^{2\prime} - 0.4884(\nabla^{2\prime})^2 \qquad (4)$$

$r^2 = 0.982$, $\sigma_{51} = 0.023-3.9\%$, $(\nabla^{2\prime\prime})_{max} = -1.475$ at $\nabla^{2\prime} = 0.117$, $\nabla^{2\prime\prime} = 0$ at $\nabla^{2\prime} = -0.985$ and -1.964, and $\nabla^2_s = -0.423$. In the $\nabla^{2\prime},(\nabla^{2\prime\prime} - \nabla^{2\prime})$ plot this translates into $r^2 = 0.999$, $\sigma_{51} \sim 1.2\%$ of the $\nabla^{2\prime\prime} - \nabla^{2\prime}$ range. A perhaps more natural *logarithmic* plot $\nabla^{2\prime\prime} - \nabla^{2\prime} = 1.073 + 1.3233 \ln(-\nabla^{2\prime})$ gives $r^2 = 0.996$, $\sigma_{52} = 0.041-2.1\%$, $\nabla^2_s = -0.445$, a result not much different for the data range. There is thus no doubt about the continuity of the two Laplacians over the entire data range and of their high degree of correlation. Furthermore, in N−H···N bonds approaching symmetric (**5**−**7**, **9a**, **9b**, **15**), i.e., for $|\nabla^{2\prime}| < 0.985$ (Figure 6), $\nabla^{2\prime\prime}$ assumes *negative* values. This must be kept in mind when using $\nabla^{2\prime\prime} > 0$ as a rule-of-thumb criterion of hydrogen bonds as closed-shell interactions (see below).

The kinetic energy densities G' and G'' are both positive, as required.[9,11] The considerable scatter in the G'',G' plot (Figure 7A) made the choice of model function uncertain, although the plot suggested a concave trend. However, a remarkable reduction of the scatter and a clear trend resulted when the *ratio* G'/G'' was plotted against G'' (Figure 7B). Although a simple power regression

$$G'/G'' = 0.0700(G'')^{-0.9197} \qquad (5)$$

($r^2 = 0.623$, $\sigma_{51} = 0.651-7.7\%$) rendered the trend reasonably well for $G'' > 0.01$ (Figure 7B, thin line), a more satisfactory fit was obtained with the function

$$G'/G'' = \exp[0.9100 + 1.0933 \ln G'' + 0.2733(\ln G'')^2] \qquad (5a)$$

$r^2 = 0.957$, $\sigma_{51} = 0.338-4.0\%$ (Figure 7B, thick line). This function has $(G'/G'')_{min} = 0.832$ at $G'' = 0.135$, i.e., well outside the data range. Expressing G' from (5a) makes it possible to draw the regression line in Figure 7A, for which $r^2 = 0.654$, $\sigma_{51} = 0.005-15\%$, $G_s = 0.0596$. The distribution of the residuals is quite uniform.

Kinetic Energy Densities K' and K''. Theory admits both positive and negative values.[9,11] In our case, $K' > 0$, but K'' can be positive or negative. When $K'' < 0$, the $|K''|$ are very small (i.e., corresponding to very weak H···N bonds) and their

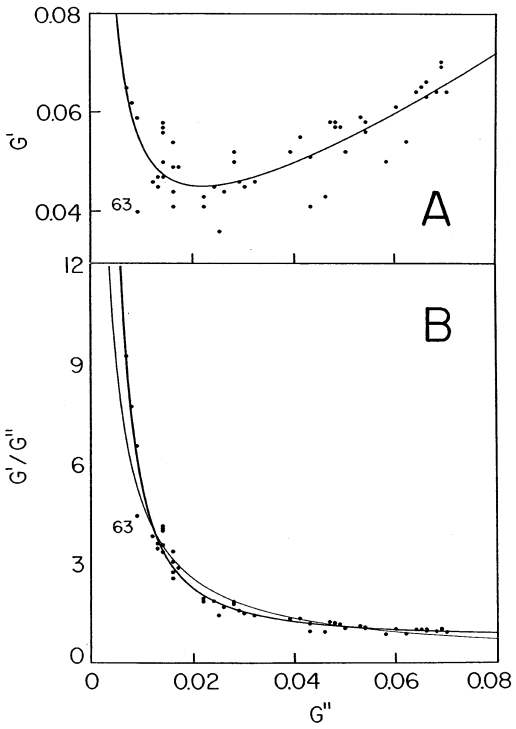

Figure 7. Correlation of the kinetic energy densities G_c. (A) Fitted curve as obtained via regression (5a). (B) Fitted curve from regression (5) (thin line) and as obtained via regression (5a) (thick line).

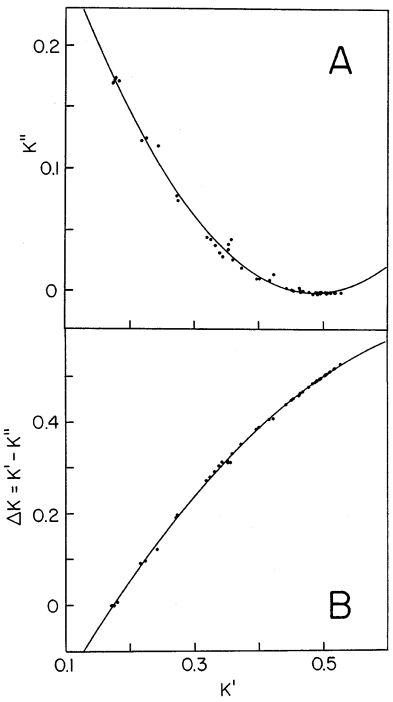

Figure 8. Correlation of the kinetic energy densities K_c. (A) Fitted curve as obtained via regression (6a). (B) Fitted curve from the quadratic regression (6).

trend is uncertain (Figure 8A). Because of their smallness we could not exclude the possibility that the K'' in fact are always positive, and that the negative K'' values are an artifact of computation. However, we have proceeded, at least initially, on the assumption that the $K'' < 0$ values are legitimate (see below).

The change of sign in K'' causes problems in the choice of model function. However, the *difference* $\Delta K = K' - K''$ is

always positive. Quadratic regression gave

$$\Delta K = -0.417 + 2.7244K' - 1.7778(K')^2 \qquad (6)$$

$r^2 = 0.999$, $\sigma_{51} = 0.0042-0.8\%$; $\Delta K = 0$ at $K' = 0.1725$ ($=K_s$) and 1.360, and $\Delta K_{max} = 0.627$ at $K' = 0.766$, i.e., well beyond the K' range (Figure 8B).

Expressing K'' from (6) gave

$$K'' = 0.417-1.7244K' + 1.778(K')^2 \qquad (6a)$$

$r^2 = 0.995$, $\sigma_{52} = 0.0042-2.4\%$; $K''_{min} = -0.0013$ at $K' = 0.485$, and $K'' = 0$ at $K' = 0.460$ and 0.510 (Figure 8A). The residuals, though small, were not distributed uniformly. The small values, at large K', are associated with weak and the large ones, at small K', with strong H···N bonds.

Potential Energy Densities V' and V'' (Figure 9S). Using the relation $V_c = (1/4)\nabla^2_c - 2G_c$ (eq 6.31 of ref 9) to calculate V' and V'', the two local potential energy densities can be related by

$$V' = -\exp[-0.541 + 4.767V'' + 4.587(V'')^2] \qquad (7)$$

$r^2 = 0.986$, $\sigma_{51} = 0.011-3.3\%$, $V' = -0.582$ at $V'' = 0$; $V'_{max} = -0.169$ at $V'' = 0.520$, i.e., well below $V_s = -0.241$. This V_s value compares well with $V_s = -0.238(4)$ calculated from the ∇^2_s and G_s values in Table 3.

More about G_c

Although the correlation between G'/ρ' and G''/ρ'' is not a proper homocorrelation, it merits being included here because of its particular and timely interest. The ratio G_c/ρ_c has been proposed[9,12,13] as a classificatory criterion for distinguishing between *types* of chemical bonds: $G_c/\rho_c < 1$ for covalent (shared-interaction) bonds, for which $\nabla^2_c < 0$; $G_c/\rho_c > 1$ for closed-shell interactions (ionic, hydrogen, van der Waals bonds), for which $\nabla^2_c > 0$. (However, see above for the variation of $\nabla^{2\prime\prime}$ with $\nabla^{2\prime}$ in N−H···N bonds close to symmetric.) It was of interest to find out to what extent the G_c/ρ_c criterion applies to the two types of bonds in the N−H···N systems in **M**.

The (G'/ρ'),(G''/ρ'') correlation is approximated by an almost purely quadratic fit

$$G'/\rho' = 0.0818(G''/\rho'')^{-2.011} \qquad (8)$$

$r^2 = 0.915$, $\sigma_{52} = 0.028-8.7\%$, $G_s/\rho_s \sim 0.435$ (Figure 10A); the *difference* is approximated by

$$G''/\rho'' - G'/\rho' = 0.9227 + 1.099\ln(G''/\rho'') \qquad (8a)$$

$r^2 = 0.981$, $\sigma_{52} = 0.028-4.1\%$, and is zero at $G''/\rho'' \sim 0.432$ (Figure 10B). For the bonds in **M**, $0.116 < G'/\rho' < 0.441$, $0.429 < G''/\rho'' < 0.804$.[14] Thus, approximately, $1 > G''/\rho'' \geq G'/\rho'$; i.e., neither ratio attains unity and, with $G''/\rho'' < 1$, the proposed criterion fails for the linear or near-linear N−H···N systems. This would indicate that the H···N bond has a substantial shared-interaction component.

A synoptic picture of the variation of G_c/ρ_c in N−H···N bonds is provided by Figure 11, where G'/ρ' and G''/ρ'' are plotted against ρ' and ρ'', respectively. The variation can be represented by

$$G'/\rho' = 0.0306(\rho')^{-1.406} \qquad (8b)$$

$r^2 = 0.931$, $\sigma_{52} = 0.0224-6.9\%$, and

$$G''/\rho'' = 0.7578 - 1.1757\rho'' - 5.9527(\rho'')^2 \qquad (8c)$$

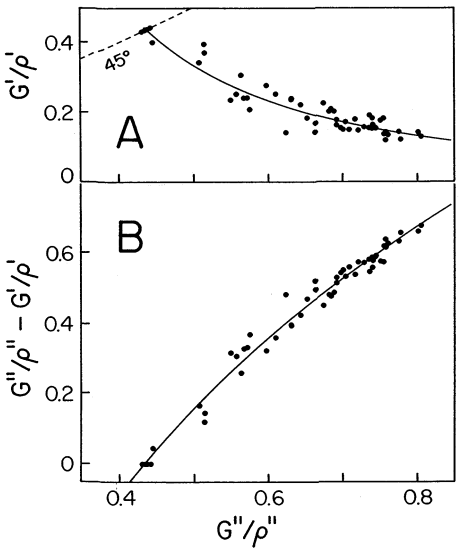

Figure 10. Variation of the ratio G'/ρ' (A) and of the difference $G''/\rho'' - G'/\rho'$ (B) with G''/ρ'' in N−H···N bonds of **M**. Fitted curve in A is from regression (8) and in B from regression (8a).

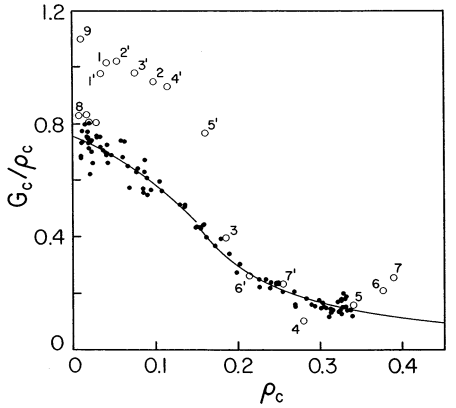

Figure 11. Complete course of G_c/ρ_c with ρ_c for N−H···N bonds of **M** (filled circles). Fitted curve for ρ',(G'/ρ') is from regression (8b) and that for ρ'',(G''/ρ'') from regression (8c). Open circles, data points for diatomic XH hydrides and other bonds in ref 9 (see text); 1−7 → X = Li−F, 1′-7′ → X = Na−Cl, 8 → Ar···HF, 9 → Ne···HF.

$r^2 = 0.872$, $\sigma_{52} = 0.039-10.4\%$, with (8b) and (8c) intersecting at $\rho'' \sim 0.145$. The plot is continuous though probably not smooth; $G''/\rho'' = 1$ cannot be reached for positive ρ''.

Abramov's Estimate of G_c. This discussion of G_c also provides an opportunity to investigate the extent of validity of Abramov's[13,15,16] estimate

$$G_c = (3/10)(3\pi^2)^{2/3}\rho_c^{5/3} + (1/6)\nabla^2_c \qquad (9)$$

of the local kinetic energy density at the BCPs of bonds between closed-shell atoms, i.e., nominally for the H···N bonds of **M**, $G''_A = 2.871(\rho'')^{1.667} + 0.167\nabla^{2\prime\prime}$.

As shown in Figure 12, G''_A approximates G'' very well for $G'' < 0.02$, i.e., for very weak H···N bonds, longer than ca. 1.9 Å (cf. Figure 13). For the 18 data points in this interval, the perpendicular deviation from the 45° line is only 0.0007−6.4% of the G'' range. Beyond $G'' = 0.02$ eq 9 progressively overestimates G'' until for $G'' > 0.06$ (i.e., for H−N···N bonds approaching symmetric) the data points scatter and the trend becomes intractable. The two most striking outliers in Figure 12A are *1* and *2*, for the symmetric bonds $[FCN-H-NCF]^+$ (**2**) and $[CN-H-NC]^-$ (**11**), respectively; the two points *3* and

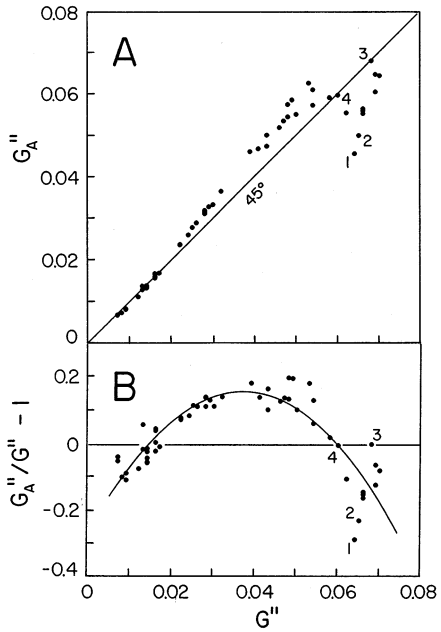

Figure 12. Comparison of Abramov's estimate of G_A'' of G'' (eq 9) with G'' for H···N bonds of **M**. (A) Direct comparison. (B) Deviation of G_A''/G'' from unity. The data points in (B) can be approximated by $G_A''/G'' - 1 = -0.266 + 22.75G'' - 307.2(G'')^2$ ($r^2 = 0.74$, $\sigma_{51} = 0.060-12\%$, $G_A''/G'' = 1$ at $G'' \sim 0.015$ and 0.060. For the identity of points *1*−*4* see text.

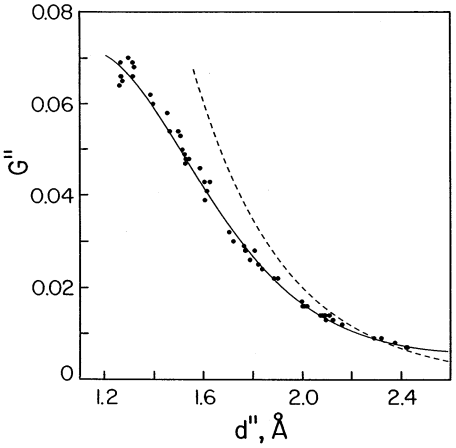

Figure 13. Correlation of G'' and d'' in N−H···N (set **M**) and O−H···O (ref 15) bonds. Fitted curve for H···N is from regression (10a) (solid line) and that for H···O from ref 15 (broken line). The d''(H···O) data set starts only at $d'' \sim 1.55$ Å.

4, approximately on the 45° line, correspond to $[F_3NH\cdots NCCN]^+$ (**9b**) and $[FNCH\cdots NCCN]^+$ (**15**). Although the progressive divergence of G''_A and G'' in Figure 12 may be due to inadequacy of the MP2/6-31G(d,p) model, it seems that its *main* cause is attributable to the limitations inherent in approximation (9).

Other Heterocorrelations Involving G_c. In their analysis of experimentally determined bond-critical parameters in X−H···O (X = C, N, O) bonds, Espinosa et al.[5,15,16] consider, among other relationships, three high correlations involving G_c (in our notation extended to H···O bonds, in au): d'',G''_A, λ_3'',G''_A, and G''_A,V''_A, and further, by extension, λ_{12}'',V''_A. These correlations have now been examined for N−H···N bonds in **M**.

The d'',G'' data set can be satisfactorily fitted by

$$G'' = 1.017 \exp(-2.047d'') \qquad (10)$$

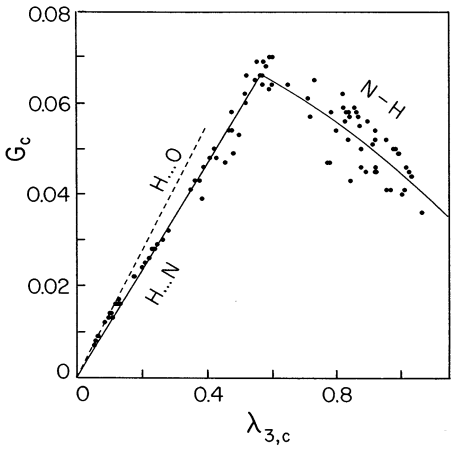

Figure 14. Complete course of G_c with $\lambda_{3,c}$ for N−H···N bonds of **M** (solid lines, expressions (10b) and (10c)) and comparison with the λ_3'',G'' regression line for H···O bonds (broken line, converted from ref 16).

$\sigma_{52} = 0.0042-6.7\%$, which corresponds to $G'' = 4.65 \exp(-2.73d'')$ for the H···O bonds (Figure 1 of ref 15, converted to au) (Figure 13). However, a significantly closer and visually plausible fit is obtained, via a $d'',\ln G''$ regression, from

$$G'' = \exp[-8.556 + 12.21d'' - 7.695(d'')^2 + 1.350(d'')^3] \qquad (10a)$$

$r^2 = 0.987$, $\sigma_{50} = 0.017-2.7\%$, with G''_{max} at $d'' = 1.13$ Å, i.e., below the d'' limit of $d_s \sim 1.26$ Å. In the d',G' plot (not shown) G' increases with d', but the large scatter prevents the data points from being meaningfully fitted. However, the composite $(d',G') \cup (d'',G'')$ plot *has a maximum* in the distribution of the data points at $d_s \sim 1.26$ Å.

The λ_3'',G'' points fall on a straight line almost passing through the origin. On constraining the regression line to pass through (0,0),

$$G'' = 0.118\lambda_3'' \qquad r^2 \sim 0.99 \qquad \sigma_{52} = 0.0023 \sim 3.7\% \qquad (10b)$$

(Figure 14). The less smooth set of points for λ_3',G' can be fitted by

$$G' = 0.080 - 0.0105\lambda_3' - 0.251(\lambda_3')^2 \qquad r^2 = 0.71$$
$$\sigma_{51} = 0.005 \sim 14\% \qquad (10c)$$

The regression lines from (10b) and (10c) intersect at $\lambda_{3,c} \sim 0.562$, in excellent agreement with the $\lambda_{3,s}$ values in Table 3. The direct proportionality of λ_3'' and G'' is consistent with the similar findings for experimental H···O bonds.[16]

The G'',V'' set of data points (Figure 15) is difficult to fit sufficiently closely to a simple function. The line for the regression

$$V'' = -\exp[-5.687 + 115.87G'' - 1755.7(G'')^2 + 14144(G'')^3] \qquad (10d)$$

for which $r^2 = 0.957$, $\sigma_{50} = 0.018-7.6\%$, does not pass through the origin, but the V'' value at $G'' = 0$ is within 1σ of the fit. This regression line practically coincides with the corresponding line for the H···O bonds (converted from ref 15) at $G'' < 0.035$, but it diverges increasingly from the latter at larger G'' values. It seems that the origin of the divergence is to be looked for

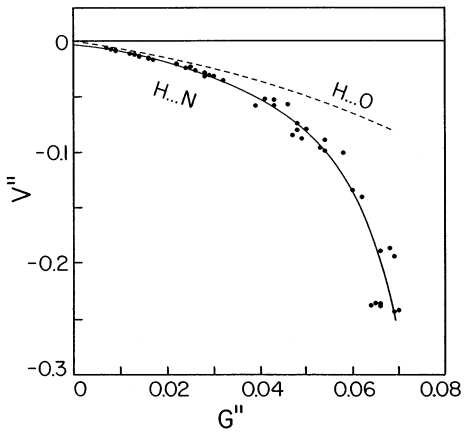

Figure 15. Variation of V'' with G'' in H···N (solid line) and H···O (broken line) bonds. The fitted curve for H···N is from eq 10d and that for H···O from ref 15; the latter ends at $G'' \sim 0.075$.

mainly in the limitations of approximation (9), which was used in ref 15 in the calculation of V''.

Closed-Shell vs Shared Interaction. It is of interest to see how the G'',V'' correlation (10d) compares with that for other nominally closed-shell interactions, specifically for the van der Waals bonds in Ne···H−F and Ar···H−F and in the three hydrogen bonds (H···O in $(H_2O)_2$ and H···N in HCN···H−F and NN···H−F), for which the bond-critical parameters are listed in Table 7.5 of ref 9; and also with the G'',V'' and related correlations for the diatomic XH (X = Li−F, Na−Cl) hydride molecules in their ground states (Tables 7.7 and A3 of ref 9). In the XH molecules Bader[9] considers the bonding interactions for X = Li,Na as closed-shell (i.e., analogous to H···N_a) and those for X = C−F,S,Cl as typical shared (i.e., analogous to N_d−H) interactions; the transition from closed-shell to shared interactions occurs earlier in the second than in the third row elements. The differences in the *type* of interaction and in the *sharpness* of the transition are manifested in his Figures 6.2, 6.3, and 7.19; they depend to some extent on the nature of the bond-critical parameter considered. In these figures the division coincides fairly clearly with (i) the change of the sign of the charge ϵ(H) on the H atom (ϵ(H) < 0 for X = Li−C, Na−S, ϵ(H) > 0 for X = N−F,Cl), (ii) the coalescence of the $\rho_c = 0.2$ au contours on X and H, and (iii) a similar coalescence of the ∇^2_c contours (Table 4).

A semilogarithmic presentation of the corresponding G_c,V_c data points (Figure 16A) immediately reveals the difference between these categories of bonds. The points for the diatomic hydrides separate into three groups. Those for XH with X = C−F (shared interaction), and those with X = Li, Be, Na−P (closed-shell interaction), each fall on an excellent straight line of their own:

$$\textbf{R1}\ (\mathrm{X = C{-}F}): \qquad \ln(-V_c) = -1.731 + 19.94G_c \qquad (10e)$$

$r^2 = 0.999$, $\sigma_2 = 0.0277{-}2.0\%$,

$$\textbf{R2}\ (\mathrm{X = Li, Be, Na{-}P}): \qquad \ln(-V_c) = -4.078 + 22.91G_c \qquad (10f)$$

$r^2 = 0.993$, $\sigma_5 = 0.072{-}1.6\%$, whereas the points for X = B, S, and Cl fall between these two nearly parallel regression lines. The points for the two van der Waals bonds and those for the three H-bonds all fall below **R2**. They are close together and at low G_c values, as expected, and without obvious separation between the two groups. Figure 16A thus again reflects, though less sharply, the difference between the closed-shell and the shared interactions, with BH, SH, and ClH as representatives of the intermediate bond character.

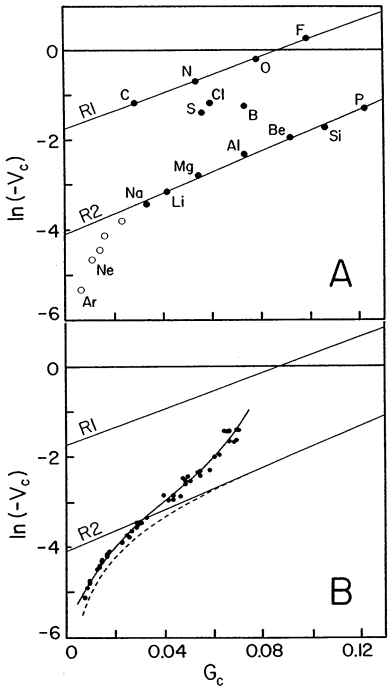

Figure 16. Correlation of V_c and G_c. (A) The data points for diatomic hydrides XH of the first and second rows (see text) are fitted by the straight lines **R1** (X = C−F, eq 10e) and **R2** (X = Li, Be, Na−P, eq 10f). The points for BH, SH, and ClH fall between **R1** and **R2**. Bader's points for the van der Waals bonds in Ar···HF and Ne···HF, and those for the three H-bonds (see text) fall below $G_c \sim 0.3$ (open circles). (B) Position of the H···N bonds of **M** (solid line) and of the H···O bonds (broken line, Figure 3 of ref 15) in plot A. The point of intersection of the H···N regression line and **R2** practically coincide with the point for NaH (the "most ionic"[9] of the XH considered here).

The division is presented in Figure 17 in terms of two other correlations, both with ρ_c as the independent parameter. The dependent parameter is the relative distance of the BCP from the H atom, $(d_{XH} - x_c)/d_{XH}$, in Figure 17A, where $d_{XH} = d$(X−H), $x_c = d$(X···BCP); and G_c/V_c in Figure 17B. The position of the transition in the correlation plots of Figures 16A and 17A,B varies somewhat with the particular choice of the two bond-critical parameters (Table 4); i.e., each combination is its own estimator of the dividing line between the two types of interaction.

The BCP in the X−H bond is closer to the X nucleus for X = Li−B and close to the midpoint of the bond for X = Na−P. In either case its position is not greatly influenced by the increasing nuclear charge on X as manifested in ρ_c (Figure 17A). However, for X = C−F and X = S, Cl the sharp discontinuity associated with the transition is accompanied by a large sudden change in the relative position of the BCP, which is now significantly closer to the proton, with d(H···BCP)/d(XH) decreasing dramatically with the increasing nuclear charge on X. These changes in the position of the BCP in the X−H bond are clearly seen in the electron-density plots of Figure 6.3 of ref 9.

The $|G_c/V_c|$ ratio for XH (Figure 17B) decreases monotonically with increasing ρ_c, the values for X = C−F converging slowly toward zero. For NaH, $|G_c/V_c| = 1$, $\rho_c = 0.0337$, i.e., nonzero; thus, $|V_c| > G_c > 0$. These trends are discussed in more detail below.

N−H···N Bonds: Closed-Shell or Shared Interactions? Of more immediate concern for the present investigation is the

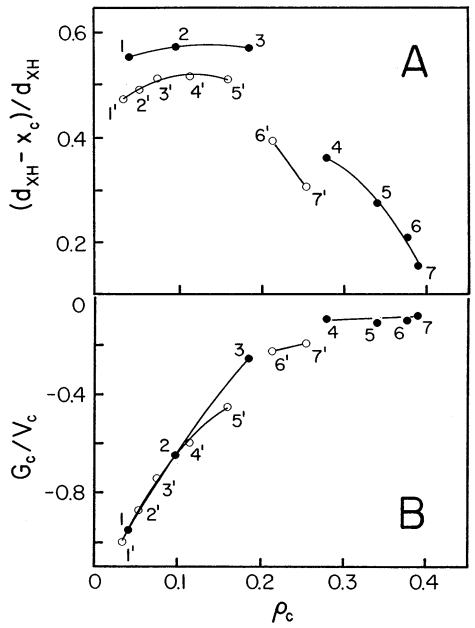

Figure 17. Separation, with ρ_c, of the bond interactions in the diatomic XH hydrides of ref 9 into shared and closed-shell, using $(d_{XH} - x_c)/d_{XH}$ (A) and G_c/V_c (B) as the classifying parameters. Filled circles, 1−7 → X = Li−F; open circles, 1′−7′ → X = Na−Cl; $d_{XH} = d$(X−H), $x_c = d$(X···BCP). See also Table 4.

position of the H···N bonds in the scheme of Figure 16A. In Figure 16B the H···N data are reasonably well accommodated by expressing ln(−V'') from (10d): $r^2 = 0.991$, $\sigma_{50} = 0.112-3.0\%$. At small G'' values the fitted curve coincides with Bader's five points (the two van der Waals and the three hydrogen bonds), but subsequently it crosses line **R2** for closed-shell interactions in XH at $G'' = 0.031$, $V'' = 0.035$, and continues toward **R1** until it ends at $G_s \sim 0.067$, $V_s \sim -0.218$, i.e., in the mixed-regime domain somewhere between G_c for BH and ClH. In other words, the amount of covalent character in H···N increases steadily until it reaches a maximum in the symmetric N−H−N bond. A similar behavior in principle is observed for the H···O bonds of refs 5 and 15. The broken line (converted from Figure 3 of ref 15) starts out more or less parallel to and somewhat below the H···N line, but with increasing G'' it practically coincides with **R2**. The lack of a sharper increase with G'' again may be due to the use of Abramov's approximation in the calculation of G'' and V'' in ref 15.

The $(\lambda_1'' + \lambda_2'')$,$V''$ correlation for H···O bonds (Figure 2 of ref 16), $V'' = 0.34(\lambda_1'' + \lambda_2'')$ (converted), is matched by the unconstrained linear correlation

$$V'' = 0.0007 + 0.2405(2\lambda_{12}'') \qquad r^2 = 0.996$$
$$\sigma_{52} = 0.0051 \sim 2.2\%$$

which is practically indistinguishable from the constrained correlation

$$V'' = 0.2394(2\lambda_{12}'') \tag{10g}$$

A slightly better visual fit at large $|\lambda_{12}''|$ is obtained with the quadratic

$$V'' = -0.0027 + 0.2077(2\lambda_{12}'') - 0.0341(2\lambda_{12}'')^2 \tag{10h}$$

($r^2 = 0.997$, $\sigma_{51} = 0.0043-1.8\%$), which generates the solid regression line in Figure 18, but as all three fits are within the

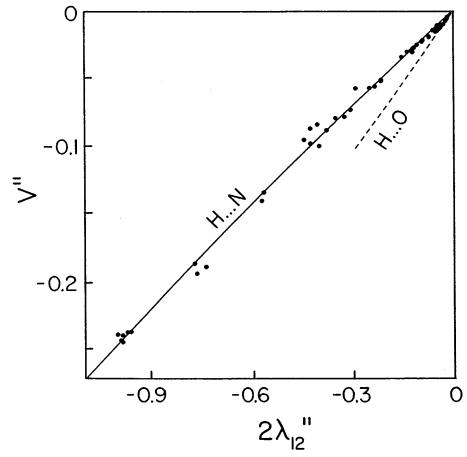

Figure 18. Correlation of λ_{12}'' and V'' (eq 10h). V'' is plotted against $2\lambda_{12}''$ to match the corresponding line for H···O bonds (dashed, see text).

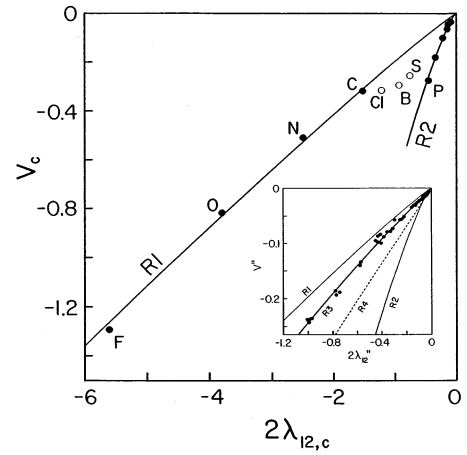

Figure 19. Correlation of $\lambda_{12,c}$ and V_c in a larger context (cf. Figure 16). Regression line **R1** (solid thin, eq 10i), XH (X = C−F); **R2** (solid thin, eq 10j), XH (X = Li, Na−P). The points for BH, SH, and ClH fall between **R1** and **R2**; BeH is omitted (see text). Inset: Enlargement of the main plot near the origin. **R3** (solid thick, eq 10h), H···N of **M**; **R4** (dashed), H···O of Figure 2, ref 16 (converted).

same statistics, the constrained linear correlation (10 g) is taken to represent the $(\lambda_1'' + \lambda_2'')$,$V''$ correlation for the N−H···N bonds of **M** adequately; i.e., V'' is directly proportional to λ_{12}'', as concluded for the H···O bonds in ref 16.

For H···N the correlation is definitely nonlinear, whereas in Figure 2 of ref 16 the H···O data points are fitted by a straight line. Keeping in mind that the $\lambda_1'' + \lambda_2''$ range of the latter may not be sufficiently wide to permit recognition of the regression function (the line ends at $\lambda_1'' + \lambda_2'' \sim -0.3$), the two regressions are in principle compatible.

A large-scale picture of the $\lambda_{12,c}$,V_c correlation emerges from Figure 19. The XH data again fall in three groups:

$$\textbf{R1}\ (\text{X} = \text{C}-\text{F}): \qquad V_c = -0.1972(-2\lambda_{12,c})^{1.0782} \tag{10i}$$

$r^2 = 0.943$, $\sigma_2 = 0.0264-2.7\%$ (quadratic regression gives a better fit even though not through the origin);

$$\textbf{R2}\ (\text{X} = \text{Li, Na}-\text{P}): \qquad V_c = -0.7166(-2\lambda_{12,c})^{1.2575} \tag{10j}$$

$r^2 = 0.897$, $\sigma_4 = 0.0087-3.6\%$. The remaining three points (BeH, SH, ClH) fall between **R1** and **R2**; the point for BeH was not included in regression (10j), as it is an unexpected and striking visual outlier that clearly does not belong in **R2**. Unlike

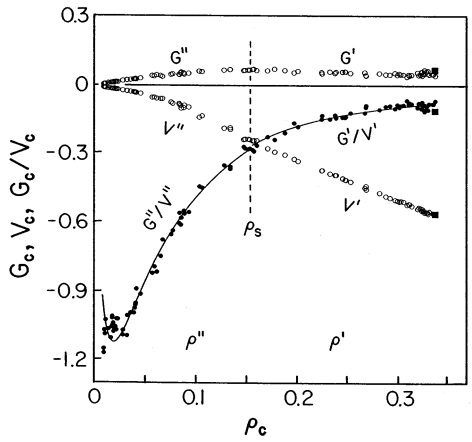

Figure 20. Correlation of G_c, V_c, and G_c/V_c with ρ_c for the N−H···N bonds of **M**. For the solid line see (13a) and text. The points for NH($^3\Sigma^-$) optimized in MP2/6-31G(d,p) (Table 5) are shown as filled squares. This plot is to be compared with Figure 17B.

in Figure 16, where the H···N points fall below **R1** but are disposed on both sides of **R2**, in Figure 19 (inset) they fall between **R1** and **R2**. The locus **R3** of the H···N points is closer to **R1** than to **R2**, indicating that the $\lambda_{12,c}$ curvatures of H···N are significantly steeper than those for the hydrides of the second row. On the scale of Figure 19 the points for the van der Waals bonds (on the **R2** line) practically coincide with the origin.

Figure 16B shows the insertion of the H···N data points into the ρ_c,ln($-V_c$) plot of Figure 16A, the object of which is to display the gradual change of the character of the H···N bond from closed-shell to partially (though appreciably) covalent. Although shown as a separate figure, Figure 20 shows a parallel insertion of H−N···N data into the ρ_c,G_c/V_c plot of Figure 17B. This figure is interesting in several aspects. The data points can be fitted as follows (only the ρ_c,G_c/V_c regression line is shown for clarity):

$$G' = 0.0306(\rho')^{-0.4061} \qquad (r^2 = 0.465,\ \sigma_{52} = 0.0065-19\%) \tag{11a}$$

significant scatter with increasing ρ';

$$G'' = -0.0011 + 0.840\rho'' - 2.554(\rho'')^2 \tag{11b}$$

$r^2 = 0.990$, $\sigma_{51} = 0.0022-3.5\%$, $G''_{max} = 0.068$ at $\rho'' = 0.164$, lines from (11a) and (11b) intersect at $\rho_c \sim 0.145$;

$$V' = 0.0304 - 1.7821\rho' \qquad (r^2 = 0.998,\ \sigma_{52} = 0.0044-1.3\%) \tag{12a}$$

$$V'' = -0.0031 - 0.3437\rho'' - 7.860(\rho'')^2 \tag{12b}$$

$r^2 = 0.996$, $\sigma_{51} = 0.0049-2.1\%$; lines from (12a) and (12b) intersect at $\rho_c = 0.156$;

$$G'/V' = -0.01635(\rho')^{-1.4942} \qquad (r^2 = 0.921,\ \sigma_{52} = 0.0135-6.3\%) \tag{13}$$

The ρ'',G''/V'' set is difficult to fit because of the visually ill-defined cluster of data points at low ρ'' values. Taking G''/V'' as the ratio of (11b) and (12b) generates the solid line in Figure 20, for which $\sigma_{48} = 0.058-6.5\%$, i.e., acceptable. However, the unexpected appearance in this curve of a minimum at $\rho'' \sim 0.02$ leaves some doubt about the appropriateness of this ratio to represent the data set with confidence at small ρ'', i.e., very weak H···N bonds. (In this connection, note the disposition of the open-circle data points[9] at $\rho_c < 0.05$ in the ρ_c,G_c/V_c plot of Figure 11).

TABLE 5: Bond-Critical Parameters in NH_4^+ (66), F_3NH^+ (67), and NH($^3\Sigma^-$)

parameter	**66**[a]	**67**[a]	NH($^3\Sigma^-$)[b]	NH($^3\Sigma^-$)[c]
d_c, Å	1.023	1.042	1.0355	[1.0379]
ρ_c	0.3331	0.3317	0.3379	0.3395
$\lambda_{12,c}$	−1.3629	−1.5195	−1.1983	−1.2399
$\lambda_{3,c}$	0.8594	1.0831	0.6523	0.8765
∇^2_c	−1.8665	−1.9559	−1.7444	−1.6034
G_c	0.0453	0.0308	0.0648	[0.053]
K_c	0.5119	0.5198	0.5009	[0.454]
V_c	−0.5566	−0.5510	−0.5656	[−0.508]
G_c/ρ_c	0.1351	0.0935	0.1918	0.157
G_c/V_c	−0.0808	−0.0563	−0.1145	[−0.105]

[a] **66**, H_3N-H^+ (T_d); **67**, F_3N-H^+ (C_{3v}); Table 4 of ref 1. [b] MP2/6-31G(d,p) optimized, this work. [c] Near HF values, ref 9. Values in brackets converted from those listed.

Figure 20 shows more clearly than Figure 17B that with increasing ρ_c the $|G_c/V_c|$ ratio converges steadily to zero. For the H···N bonds the decrease in $|G''/V''|$ is substantial. The V' range is about 10 times that of G'. Furthermore, the increase of $|V'|$ with ρ' is *linear*, with very small scatter (cf. eq 12a). The G' values decrease with increasing ρ' almost linearly but with a significant scatter, which increases with ρ'. The MP2/6-31G-(d,p) values of ρ_c, G_c, V_c, and G_c/V_c in the diatomic NH($^3\Sigma^-$) (Table 5) provide satisfactory terminating points for the three data sets, fully consistent with the respective data-point sequences of Figure 20. This confirms that the N−H bond in the N−H···N system is not different in character from other covalent N−H bonds.

The plots of Figure 20 are a good illustration of the correlated behavior of the potential and kinetic energy densities in the N−H bonds. With increasing ρ' the potential energy density V' at the BCP increases, consistent with the increasing number of electrons coexisting in a unit space element at the BCP and with the Pauli principle; for ρ',V' this increase is linear. At the same time the increased ρ' (and thus V') progressively restricts the kinetic freedom of these electrons, which is reflected in a decrease in G'. However, with increasing ρ', G' decreases more slowly than $|V'|$ increases, resulting in the convergence of $|G'/V'|$ toward zero.[17] Analogous behavior is observed for the H···N part of Figure 20 except that the variation of G'' and V'' with ρ'' is not linear; that of V'' with ρ'' seems to merit further examinations when additional (or improved) data become available.

Last we add that the homocorrelation $|G'/V'|$,(G''/V'') (not shown) can be represented by $G''/V'' = -0.0698(-G'/V')^{-1.1065}$, $r^2 = 0.998$, $\sigma_{52} = 0.123-13.8\%$, $G''/V'' = -G'/V'$ at $|G_s,V_s| = 0.284$. There is increasing scatter of the data points for $|G'/V'| < 0.1$.

Discussion

Ideally, one would wish for acceptable expressions for optimum homocorrelations that can be obtained directly in an explicit form, $p' = f(p'')$ or $p'' = f^{-1}(p')$. Although such a description may occasionally be found, in the absence of theory, one generally has to settle for the best analytical approximation to the data set that can be found empirically. No effort was made to discover such direct functions beyond the attempts described above. As for the results of these attempts, it is striking to encounter such a diversity of p',p'' and p'',p' variation as that in the preceding section, ranging as it does from a linear relationship between ρ' and ρ'' to nonmonotonic variation in other cases.

The ρ'',ρ' homocorrelation (1) is the only one of those examined that is linear over the N−H···N data range, $d\rho'/d\rho'' = -1.3$. From (1) it follows that the sum of the electron densities at the two BCPs, $\rho' + \rho'' = 0.3506 - 0.302\rho''$, is not constant but decreases linearly with increasing ρ''. It is a minimum at $\rho_s = 0.152$ and a maximum at the $\rho'' = 0$ limit, in good numerical agreement with ρ_c in the MP2-optimized NH($^3\Sigma^-$) (cf. Figure 20).

Attempts to find satisfactory explicit regression functions were at times frustrated by the considerable scatter in the correlation plot (cf. Figures 1A, 4A, and especially 7A). The p' parameters in general scatter more than the corresponding p'', possibly because MP2/6-31G(d,p) describes the H···N part of the N−H···N bond more adequately than it describes the covalent N−H part, the higher electron density in the latter requiring a more complete account of the inter-electron interactions than MP2/6-31G(d,p) can provide. It was often correlations involving p'/p'' or p''/p' ratios or $|p' - p''|$ differences, rather than p', p'' as such, that were monotonic and represented the data set with a high degree of fidelity. It therefore seems that it is those indirect correlations that are the most useful in uncovering trends and tend to be statistically more satisfactory: cf. for example, Figures 4 and 7.

From eqs 5.49 and 6.31 of ref 9 it follows that $K_c + G_c + V_c = 0$, $G_c \geq 0$, $V_c \leq 0$, which implies that K_c is negative when $|V_c| > G_c$. The closeness of approximation (7) (and of other approximations not reported here) to the data set would suggest that the $K'' < 0$ values are in fact legitimate and not artifacts of computation; i.e., at d'' larger than ∼1.77 Å (N···N = D larger than ∼2.8 Å) K'' can assume small negative values that, with increasing d'', converge to zero from below (Figure 8A).

Because of the internal self-consistency of the homocorrelations the bond-critical parameter values p_s in symmetric N−H−N bonds can be estimated by utilizing the *entire* p_c data set rather than only the information from individual symmetric N−H−N bonds. This is particularly useful, as extraction of p_s values from experimental electron densities in symmetric X−H−X bonds is not without difficulties and confirmation from calculation is desirable (cf. part 1 for a discussion of this point). In Table 3 the p_s values obtained from the homocorrelations are compared with the means computed from the p_s values in the five symmetric bonds (**2**−**4**, **10**, and **11**) in Table 4 of part 1.

Inferences from statistics (i.e., from high degree of correlation) almost certainly imply the existence of *functional* dependence, the formal expression of which must be looked for not merely in phenomenology but in more developed theory. In ref 16 it is specifically suggested that (in our notation) the curvatures λ_i'', G'', and V'' in X−H···O bonds described from experiment are quantities intrinsically related. In this paper and in part 1 we show, on numerous examples of N−H···N bonds, that relationships of this kind exist not only between disparate bond-critical parameters p'',q'' in the H···N portion of a complete bond, but, more globally, between the conjugate parameters p' and p'', i.e., in the N−H···N *systems*; and that, generally, in p_c,q_c plots correlating p',q' *and* p'',q'' in the N−H···N bonds the two sets of data points cannot be represented by a single, smooth ($p_c = p' \cup p''$), ($q_c = q' \cup q''$) global regression line but require separate regression lines, one for p',q', another for p'',q''. These regression lines intersect at the p_s,q_s point for symmetric N−H−N bonds, reflecting the different character of the N−H and the H···N bonds. It is likely that this finding applies to X−H···X bonds in general. In the case of mixed X−H···Y bonds, the nonequivalence of the donor and acceptor atoms of course imparts to the X−H and H···Y bonds different characters *ipso facto*.

Conclusions

The geometries of 54 small molecular species containing linear or near-linear N−H···N bond systems have been optimized at the MP2/6-31G(d,p) level and the values of the bond-critical parameters $p_c = \rho_c$, $\lambda_{i,c}$, ∇^2_c, G_c, K_c, and V_c at the BCP computed (sample **M**). In each N−H···N system the parameters p' refer to the N−H and the p'' to the H···N bond. Detailed examination of these parameters demonstrates that in each such system the conjugate p' and p'' are highly correlated, and furnishes a consolidated picture of the parameter trends as well as a self-consistent set of numerical p_c values at the symmetric N−H−N limit.

The p' parameters in general scatter more than the corresponding p'' parameters, possibly because the MP2/6-31G(d,p) optimization scheme describes the H···N part of the N−H···N system more accurately than it describes the N−H bond, the latter being essentially covalent and thus having higher electron density, which imparts greater importance to electron-correlation interactions. If p' and p'' each show significant scatter but $|p' - p''|$ or p''/p' do not, this is proof that the computations for the individual entries in **M** are correct, and that the scatter in p' and p'' is due to "chemical" variation in the data set.

The N−H and the H···N bond in an N−H···N system do not have the same character, so that, for example, the variation of a parameter p' with ρ' and that of p'' with ρ'' cannot, in principle, be represented by the same regression function. The parameter values develop steadily from very weak N−H···N to symmetric N−H−N bonds. In the latter the character of the bond interaction is appreciably covalent, with $\nabla^2_c < 0$ (Figure 6) and $G_c/\rho_c < 1$ (Figure 11). Thus neither the sign of ∇^2_c nor that of $G_c/\rho_c - 1$ is a reliable criterion of the type of bond interaction (closed-shell or shared) in medium and strong N−H···N bonds. Comparison of the bond-critical parameter values in **M** with Bader's[9] HF values for diatomic XH molecules makes it possible to position the range of strength of the N−H···N bonds in the overall scheme of X−H bond interactions (Figures 11, 16, 19, and 20). This calibration of the N−H···N strength would undoubtedly improve if the p_c values for the XH hydrides were recalculated at the MP2 level.

Abramov's[13] approximation (9), designed to estimate G_c in bonds between closed-shell atoms from experimental values of ρ_c and ∇^2_c, is shown to represent the G'' values in the H···N bonds in **M** very well up to $G'' < 0.02$ au, i.e., for very weak H···N bonds with $d'' = d(\text{H}\cdots\text{N}) > 1.9$ Å.

The extreme paucity of reliable experimental values of p' and p'' precludes extensive direct comparison with **M**. However, such experimental values of ρ_c and ∇^2_c as exist[18,19] indicate better than semiquantitative agreement with **M** even in severely bent N−H···N bonds or when the underlying position of the proton is not accurately known. It is, however, noted that the *distance* relationships in the N−H···N bonds of **M**, when confronted with values obtained from neutron diffraction, are in good agreement (cf. part 1). It is also reassuring to find that G'' in the ab initio set **M** is directly proportional to λ_3'' (eq 10b) and V'' to λ_{12}'' (eq 10 g): this parallels the corresponding findings reported in refs 15 and 16 for the *experimentally* determined parameters in H···O bonds.[20]

Acknowledgment. We thank Dr. T. S. Cameron for his comments on the manuscript and Dr. E. Espinosa for clarifying certain points in refs 5, 15, and 16. Special thanks are due to

Dr. K. N. Robertson for her assistance with the preparation of the figures. Financial support from the Natural Sciences and Engineering Research Council of Canada is acknowledged.

Supporting Information Available: Figure 5S (correlation of the $\lambda_{3,c}$ curvatures; fitted curve from regression (3b)) and Figure 9S (correlation of the potential energy densities V_c). This material is available free of charge via the Internet at http://pubs.acs.org.

References and Notes

(1) Knop, O.; Rankin, K. N.; Boyd, R. J. *J. Phys. Chem. A* **2001**, *105*, 6552.

(2) Errata for part 1. Page 6558, Table 4, entry **53**, second line: read −0.0233 instead of −0.0333. Page 6564: eq 8f, read ln ρ'' instead of ln ρ; read 0.998, instead of 0.998.; read ln d'' instead of ln d'.

(3) Steiner, T. *J. Chem. Soc., Chem. Commun.* **1995**, 1331.

(4) Ramos, M.; Alkorta, I.; Elguero, J.; Golubev, N. S.; Denisov, G. S.; Benedict, H.; Limbach, H.-H. *J. Phys. Chem. A* **1997**, *101*, 9791.

(5) Espinosa, E.; Souhassou, M.; Lachekar, H.; Lecomte, C. *Acta Crystallogr.* **1999**, *B55*, 563.

(6) Alkorta, I.; Elguero, J. *Struct. Chem.* **1999**, *10*, 157.

(7) O'Brien, S. E.; Popelier, P. L. A. *Can. J. Chem.* **1999**, *77*, 28.

(8) Alkorta, I.; Barrios, L.; Rozas, I.; Elguero, J. *J. Mol. Struct. (THEOCHEM)* **2000**, *496*, 131.

(9) Bader, R. F. W. *Atoms in Molecules: a Quantum Theory*; Clarendon Press: Oxford, U.K., 1990.

(10) Coppens, P. *X-ray Charge Densities and Chemical Bonding.* International Union of Crystallography, Oxford University Press: Oxford, U.K., 1997.

(11) Tal, Y.; Bader, R. F. W. *Int. J. Quantum Chem: Quantum Chem. Symp.* **1978**, *12*, 153.

(12) Bader, R. F. W.; Essén, H. *J. Chem. Phys.* **1984**, *80*, 1943.

(13) Abramov, Yu. A. *Acta Crystallogr.* **1997**, *A53*, 264.

(14) The estimate of G_c/ρ_c in NH($^3\Sigma^-$) in Bader's Table 7.7 is 0.157.[9] The G_c/ρ_c values for the ground-state XH = CH, NH, OH, FH in that table vary linearly with the number n of p electrons in the X atom: $G_c/\rho_c = -0.094 + 0.050n$, $r^2 = 0.997$, $\sigma = 0.004$−3% of range.

(15) Espinosa, E.; Molins, E.; Lecomte, C. *Chem. Phys. Lett.* **1998**, *285*, 170.

(16) Espinosa, E.; Lecomte, C.; Molins, E. *Chem. Phys. Lett.* **1999**, *300*, 745.

(17) The relationship between G_c and V_c for H···O has been interpreted in ref 15 in somewhat different but fundamentally similar terms.

(18) Robertson, K. N. Doctoral Thesis, Dalhousie University, 2001.

(19) Mallinson, P. R.; Wożniak, K.; Smith, G. T.; McCormack, K. L. *J. Am. Chem. Soc.*, **1997**, *119*, 11502.

(20) The implications of these heterocorrelations will be discussed in detail in part 3.